JOURNAL OF MATERIAL SCIENCE 29 (1994) 5852–5858

Microstructure and tensile properties of AISI 316 stainless steel electron-beam cladded on C40 mild steel

S. TOSTO, F. NENCI, HU JIANDONG*
ENEA CRE Casaccia, Via Anguillarese 301, 00060 Roma, Italy

A 60 kV electron-beam equipment was used to clad an AISI 316 stainless steel plate on C40 plain carbon steel. A homogeneous coating of stainless steel was obtained. The microstructure of the clad layer consisted of delta-ferrite, austenite, M_6C carbide and martensite twinned on 1 1 2 crystal faces. The austenite has a heavily dislocated substructure and is characterized by intrinsic stacking faults. The crystallographic relationship between austenite and martensite was consistent with the Kurdjumov–Sachs relationship:

$$\{1\,0\,1\}\ \text{martensite} \| \{1\,1\,1\}\ \text{austenite}$$

and

$$\{1\,1\,1\}\ \text{martensite} \| \{1\,0\,1\}\ \text{austenite}$$

M_6C and austenite followed a relationship such as

$$(1\,1\,0)\ M_6C \| (1\,1\,0)\ \text{austenite}$$

and

$$(1\,1\,1)\ M_6C \| (1\,1\,1)\ \text{austenite.}$$

1. Introduction

Interest has been recently addressed to laser- and electron-beam alloying and cladding [1–3]. Industrial applications have also been exploited in some cases. Laser surface processing is usually carried out by injecting the powders to be cladded or alloyed on to the molten surface of the substrate under irradiation; the remixing of the molten pool enables the chemical composition and microstructure of the substrate to be modified. This procedure is rather difficult in the case of electron-beam (EB) treatments. Previous work [4–6] has shown that the irradiation of a bilayer "AISI 316 stainless steel/C40 mild steel" enables a variety of surface chemical compositions and microstructures to be obtained; the main parameters controlling the final dilution of the alloy elements of the stainless steel in the molten pool are the power and interaction time of the beam and the thickness of the overlayer sheet. The results have shown a corrosion resistance of the coated mild steel equal to that of the original stainless steel [5]. The microstructure markedly depends on the EB processing parameters and the thickness of the original AISI 316 stainless steel used for coating [6]. The dilution can be carefully controlled because the overlayer melts and wets the substrate, thus facilitating the heat contact necessary for a homogeneous cladding or alloying process. The solidification of the molten alloy is a complex process and depends on its chemical composition. The purpose of this work was to investigate, using transmission electron microscopy (TEM), the microstructure of the clad layer after solidification, in particular near to the liquid/solid interface at the melt depth.

2. Experimental procedure

The clad material was an AISI 316 stainless steel sheet having a size of 100 mm × 35 mm × 2 mm. Its chemical composition is given in Table I. The substrate material was a plain carbon steel C40 with a carbon content of 0.4 wt%. The AISI 316 stainless steel plate was mechanically clamped on to the substrate and mounted on an x–y table and irradiated with a travel speed of 20 cm min^{-1}. A line source was obtained scanning the beam at a frequency of 1000 Hz normal to the travel direction. The treatment parameters were as follows: accelerating voltage of the electron beam 60 kV, beam current 110 mA, scanning width 25 mm. The resulting width and depth of the clad layer were 25 and 3.5 mm, respectively. X-ray diffraction, SEM and microanalysis were used to examine and identify the phases formed. The surface microhardness was determined

* Permanent address: Microanalysis Center, Jilin University of Technology, Changchun, 130025, China.

0022–2461

TABLE I Chemical composition (wt %) of AISI 316

	Ni	Cr	Ti	Mo	Si	S	Mn	Cu	P	C
Wt %	13.2	17.7	0.034	2.71	0.72	0.005	1.04	0.22	0.03	0.03

with a microhardness tester. The coated sample was machined to obtain a tensile specimen whose geometry is reported in Fig. 1. For comparison, a tensile specimen was also obtained from the untreated C40 steel. Three slices parallel to the coated surface were obtained at different depths for TEM observation. Thinning of each slice was carried out using a series of SiC grinding papers and then a twin-jet polisher. The thinning solution consisted of a 5% perchloric acid and ethanol at a temperature of about − 15 °C; the thinning voltage and current were 60 V and 100 mA, respectively. The TEM observations were carried out with a JEM-400FX instrument operated at 400 kV.

3. Results and discussion

3.1. Microstructure of the clad layer

The AISI 316 stainless steel plate was fully melted under the given irradiation conditions. SEM observations and X-ray diffraction have shown that the coated layer is composed of f c c austenite, b c c ferrite/martensite and carbide. No porosities nor microcracks were observed on the metallographic cross-section. The Mössbauer spectra [4] enabled us to determine that the volume content of the f c c phase was 5%, carbide 3% and b c c phase balance. The interface between the coated layer and unmelted region was found at a depth of about 3.5 mm, i.e. shifted towards the C40 steel with respect to the initial thickness (2 mm) of the sheet of stainless steel. Then, a small amount of substrate was also melted under the given irradiation conditions. As previously found [6], the distribution of nickel, chromium, titanium and iron is homogeneous in the clad layer, but the content of these elements is slightly diluted with respect to the initial composition of the stainless steel; the dilution factors for both chromium and nickel under these experimental irradiation conditions are estimated to be about 0.6.

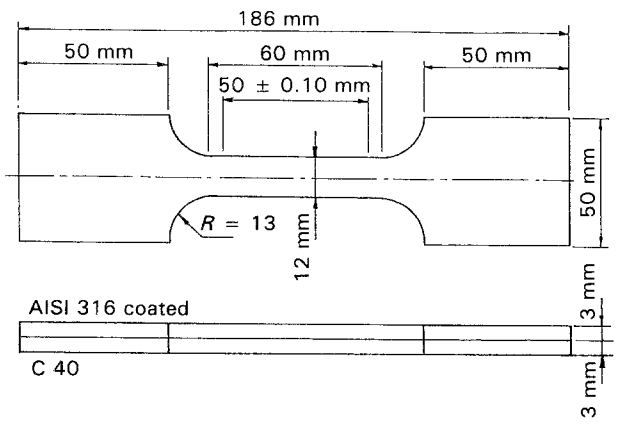

Figure 1 Geometry of the tensile specimen.

3.2. Microhardness of the clad layer

Fig. 2 shows the microhardness profile as a function of depth in the clad layer. The values of microhardness are fairly constant but increase sharply near the interface with the substrate. The TEM reveals that this region is characterized by the presence of twinned martensite, in agreement with the local increase of hardness. It can be explained by the diffusion of carbon from the substrate towards the clad layer. The microhardness of the clad layer is higher than that of the original AISI 316. According to published papers, the increment is due to a fine microstructure of the alloyed ferrite; this latter was formed because of the enhanced solubility of the alloy elements of AISI 316 during rapid cooling [4].

3.3. Tensile tests

The results of the tensile tests are shown in Table II. As can be seen, the bilayer specimen consisting of the clad AISI 316 and C40 substrate has improved properties compared with the untreated substrate. SEM observations on the fracture surface, reported in Fig. 3a–c, reveal different fracture mechanisms. The clad layer of AISI 316 is characterized by the presence of small dimples, typical of a ductile crack propagation. Microcracks were found on the C40 side, where

TABLE II Tensile properties of the coated specimen: ultimate tensile strength (UTS), yield strength (YS), necking (A%) and rupture stain (L%)

	UTS (N mm^{-2})	YS (N mm^{-2})	(A%)	(L%)
EB coated materials	906	399	82.1	8
C40	644	629	62.2	14

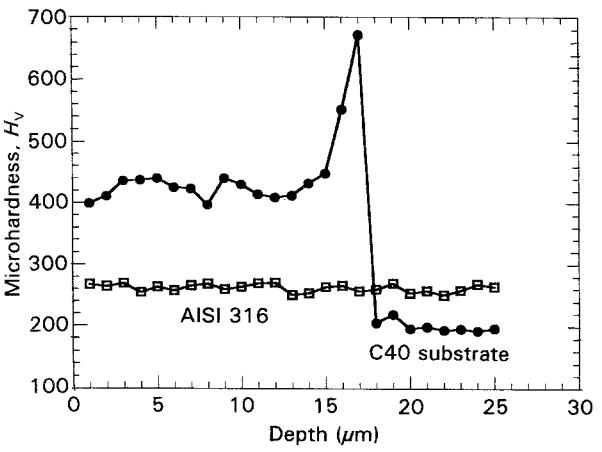

Figure 2 Microhardness versus distance. for (●) EB treated and (□) untreated samples.

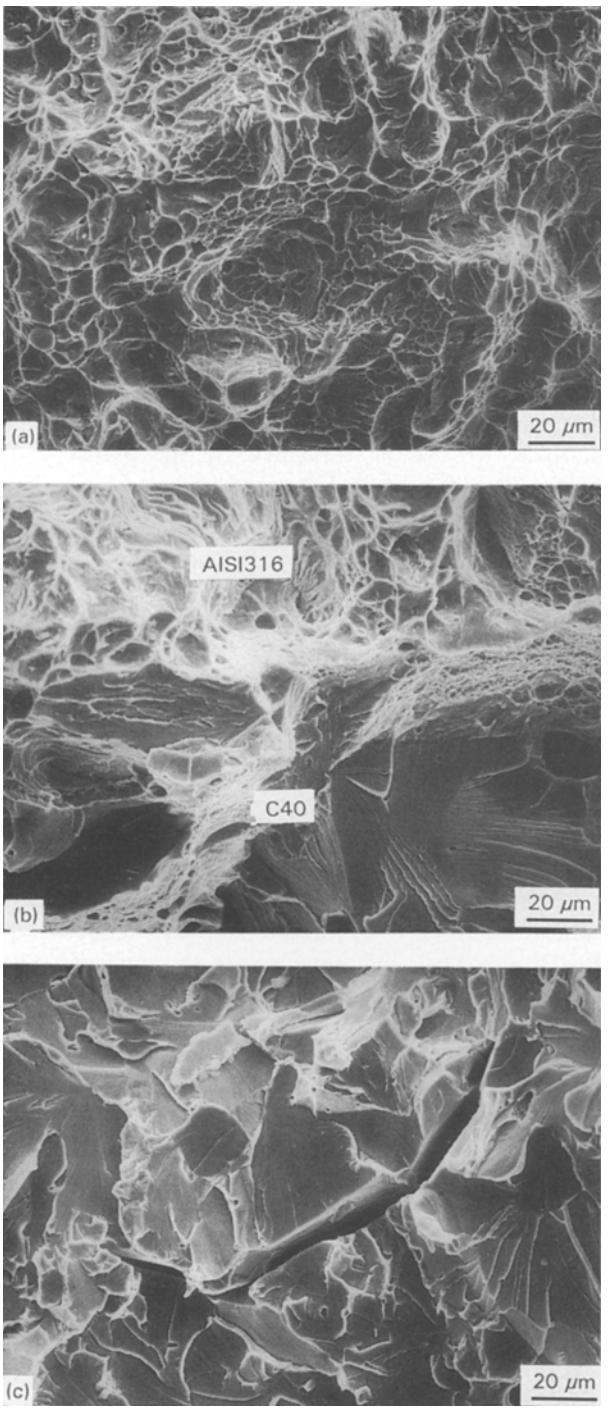

Figure 3 Scanning electron micrographs showing the morphology of the fractured surface: (a) coated layer; (b) interface; (c) C40 substrate.

the crack propagates by cleavage. No microcracks were noted at the interface between the clad AISI 316 layer and the substrate. This indicates that a good adhesion was obtained as a consequence of EB irradiation. The element diffusion across the interface is the reason for the adhesion between the clad layer and substrate. The brittleness of C40 carbon steel is due to the occurrence of quenching and partial tempering because of irradiation. This is because the melting of AISI 316 causes heat diffusion towards the substrate and then the heat treatment of this latter.

3.4. TEM observations

30 thin foils taken from different depths were observed

Figure 4 Transmission electron micrograph showing the austenite solidified from the molten phase. Stacking faults and dislocations are visible.

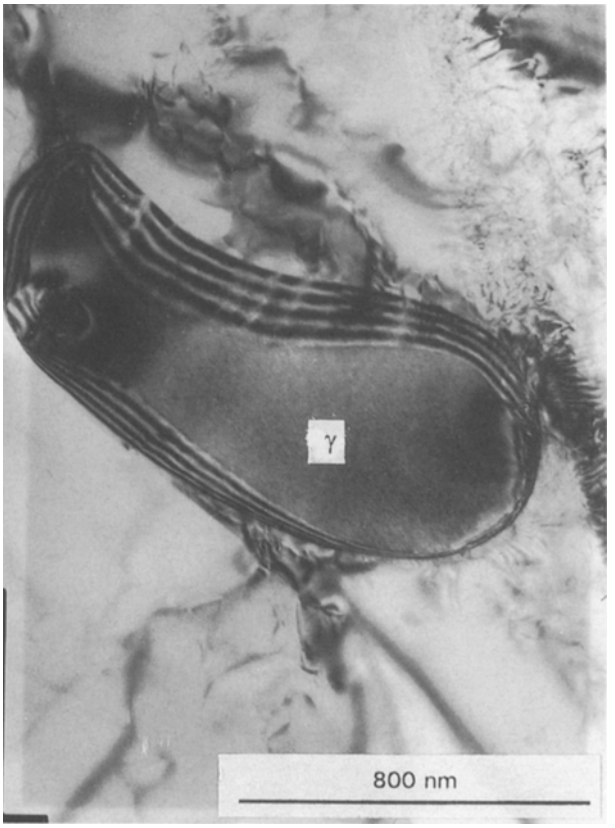

Figure 5 Transmission electron micrograph, showing austenite with a round boundary.

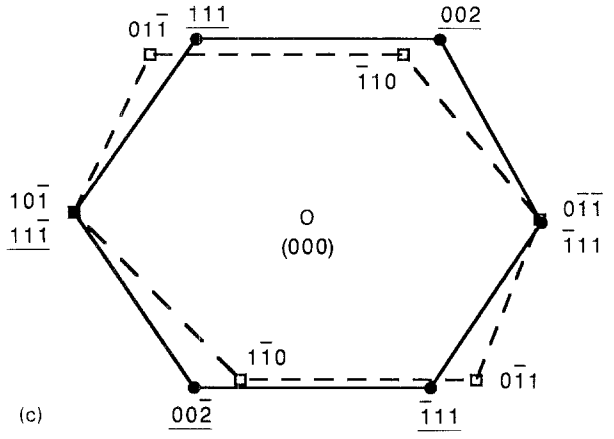

Figure 6 Transmission electron micrographs showing (a) martensite and austenite, (b) the electron diffraction pattern of martensite and austenite, and (c) pattern indexing of (b). (–●–) [1 1 0] austenite, (- - □ - -) [1 1 1] martensite.

by TEM. Selected-area electron diffraction was used to identify the various structures. The clad layer consists of M_6C precipitates, delta-ferrite, austenite and alpha-martensite. The delta-ferrite formed from the molten phase was often identified by its round boundaries, containing a relatively high dislocation density. There are two kinds of austenite with different morphology in the clad layer; both are characterized by the presence of stacking faults in a heavily dislocated substructure (see Fig. 4). The stacking faults were identified to be of intrisic type using the technique discussed elsewhere [11]. One form of austenite has round boundaries, as shown in Fig. 5, and different sizes. This austenite was formed directly from the molten phase. The other is usually bounded by martensite; it suggests that it is due to a partial transformation of the austenite grain boundary to martensite during cooling. Fig. 6 shows the morphology of austenite and martensite. The boundaries between these phases are straight lines; their directions change to form steps (see Fig. 6a). It agrees with the fact that the transformation from austenite to martensite follows a diffusionless (athermal) mechanism. The electron diffraction patterns and indexing are shown in Fig. 6b and c, respectively. It can be seen that there is a Kurdjumov–Sachs(K–S) relationship between austenite and martensite, i.e.

$$\{1\,0\,1\}\ \text{martensite} \| \{1\,1\,1\}\ \text{austenite}$$

and

$$\{1\,1\,1\}\ \text{martensite} \| \{1\,0\,1\}\ \text{austenite}$$

Fig. 7a shows the twinned structure of martensite; Fig. 7b is the dark-field image of Fig. 7a. The electron pattern and indexing are shown in Fig. 7c and d, respectively. It can be seen that the twinning crystal plane is $\{1\,1\,2\}$. It is interesting to note that austenite is also visible in Fig. 7a; the arrow indicates the stacking faults present in austenite. Some of the twinned martensite crystals lay regularly on the austenite boundaries (see Fig. 8). It suggests that they were nucleated on the grain boundary and then grew towards the inside of the grain along the preferred crystallographic direction. Most of the martensite was formed as round grains and a few laths preferentially near the interface. The formation of the martensite is thought to be related to a relatively high carbon content diffusing from C40 to the molten phase. Epsilon-martensite was not found in the clad layer; only few precipitates were observed. Fig. 9a shows the morphology of one of

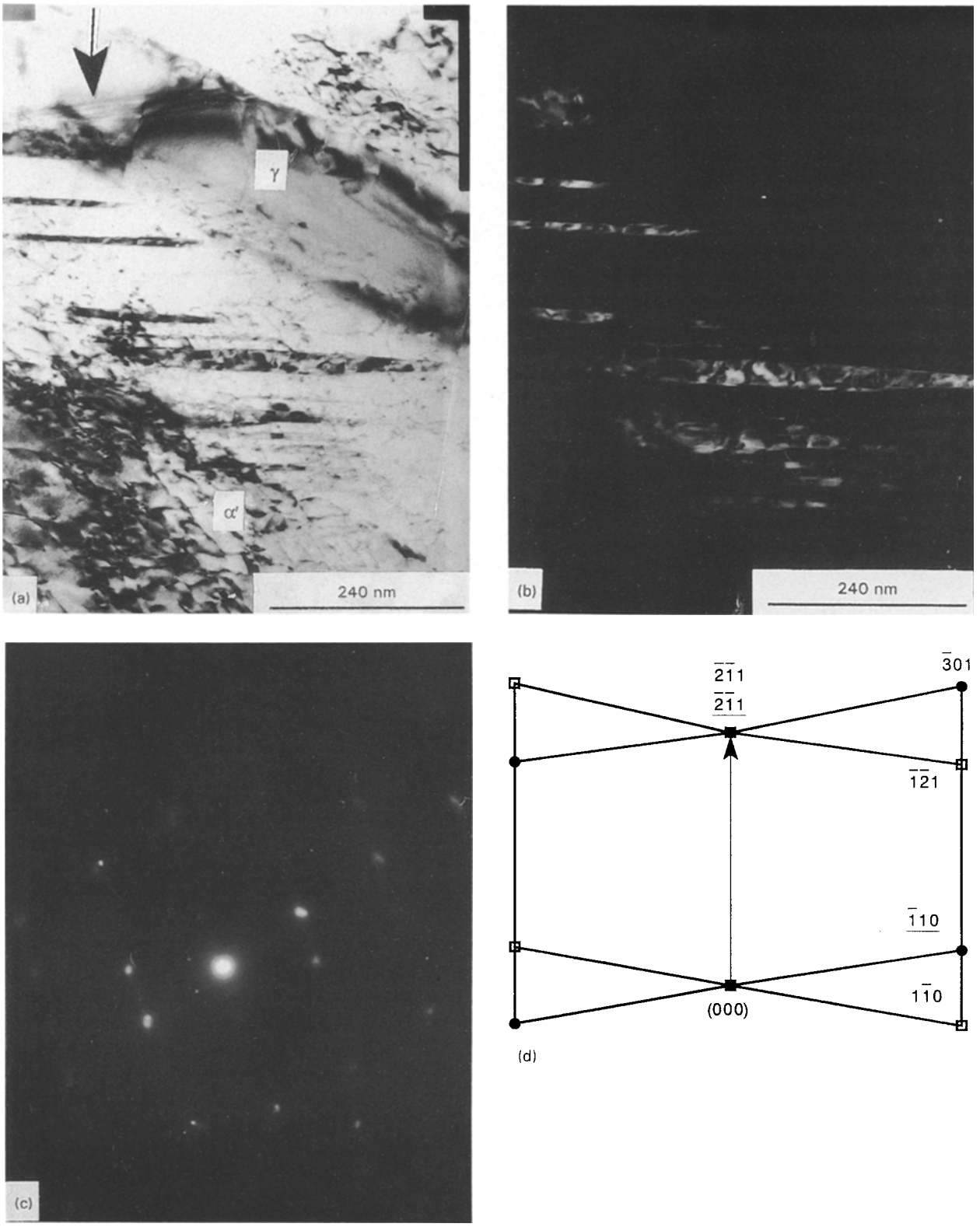

Figure 7 Transmission electron micrographs showing the twinned martensite: (a) bright field, (b) dark field, using a twin spot (1 1 0) to obtain the image, (c) electron diffraction pattern of the twinned structure, (d) indexing of (c): (–●–) [1 1 3] martensite, (–□–) twin.

these precipitates. A series of electron diffraction patterns was obtained by tilting the specimen holder stage. One of them, shown in Fig. 9b, is indexed in Fig. 9c. It shows that the structure of the precipitate is similar to M_6C, in agreement with the results of X-ray diffraction (a = 1.1082 nm for f c c). These precipitates are embedded in the austenite. As can be seen in Fig. 9c, the crystallographic relationship between M_6C and austenite is as follows

$$(1\,1\,0)\ M_6C \parallel (1\,1\,0)\ \text{austenite}$$

and

$$(1\,1\,1)\ M_6C \parallel (1\,1\,1)\ \text{austenite}$$

Then, close-packed planes of M_6C and austenite are faced. The diffraction spot of austenite (1 1 1) is overlapped with that of M_6C (3 3 3) because they have a similar cell parameter: that of austenite (1 1 1) is 0.2070 nm, that of M_6C (3 3 3) is 0.2040 nm. The secondary M_6C precipitates have a round boundary and a relatively larger average size (200 nm) than the

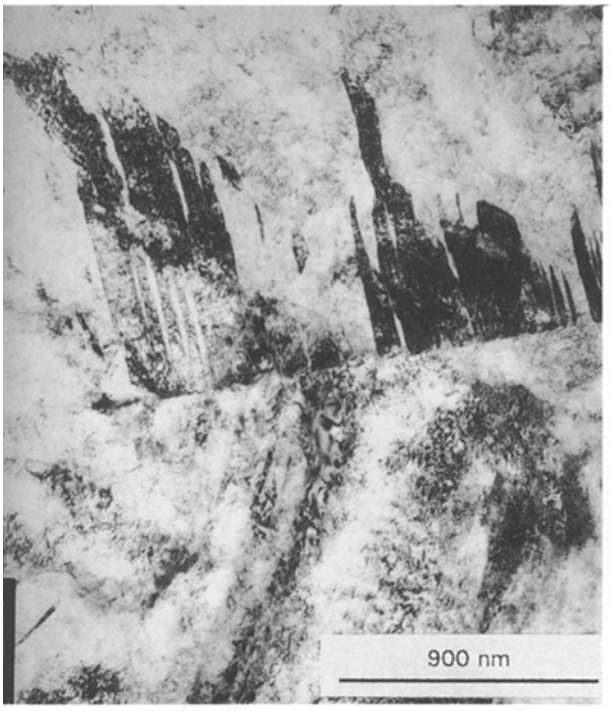

Figure 8 Transmission electron micrograph showing the twinned structure grown on the interface.

primary ones. Thus, it is deduced that these precipitates were nucleated and grown from the molten phase. In Fe–Ni–Cr stainless steel the transition from austenite to martensite involves the intermediate epsilon-martensite through the steps austenite → epsilon-martensite → b c c martensite [12]. For the transformation from austenite to epsilon-martensite, the close-packed atom planes of austenite and martensite are as identified above.

4. Conclusions

1. A clad layer of 3.5 mm was obtained from an original thickness of 2 mm of AISI 316 sheet deposited on a substrate of C40 mild steel. The profile of the interface has a zig-zag morphology and a chemical composition intermediate between that of the clad material and substrate. The ductility of the coated C40 steel is better than that of untreated C40 steel.

2. The clad layer consists of primary alpha-ferrite, austenite and M_6C. The austenite contains stacking faults and glissile dislocations. The martensite formed from austenite near the interface is in agreement with the K–S relationship. The M_6C precipitates are formed in the austenite phase according to well-established crystal relationships.

Acknowledgements

The authors thank M. Vittori, A. Montone and S. Bellini for their help during TEM observations.

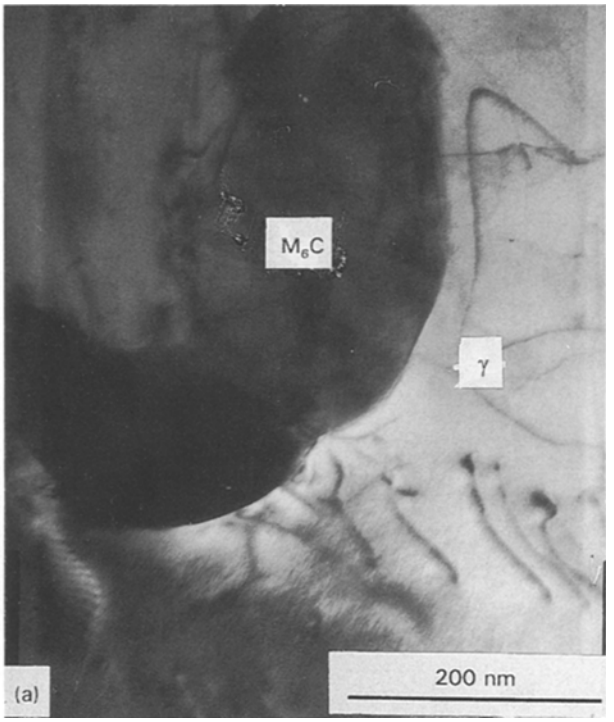

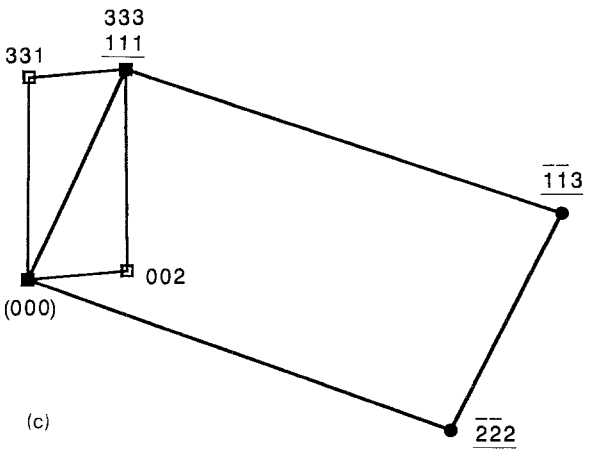

Figure 9 Transmission electron micrographs showing the M_6C carbide: (a) morphology of M_6C, (b) electron diffraction pattern, (c) indexing of (b): (–●–) $[\bar{1}\,1\,0]$ austenite, (–□–) $[\bar{1}\,1\,0]$ M_6C.

References

1. J. DE DAMBORENEA and A. J. VAZQUEZ, *J. Mater. Sci.* **28** (1993) 4775.
2. S. TOSTO, P. VANHILLE and C. VIGNAUD, *Surf. Coat. Technol.*, **53** (1993) 137–42.
3. LI YULONG and HU JIANDONG, *Proc. Adv. Mater.* **1** (1991) 193.
4. F. GAUZZI, G. PRINIPI and S. TOSTO, in "Proceedings of the 2nd European Conference on Advanced Materials and Processes", Vol. 1, edited by T. W. Cline and P. J. Withers (Institute of Materials, London, 1991) pp. 92–9.
5. C. VIGNAUD, L. BEAUNIER, A. LABARBERA, A. MIGNONE and S. TOSTO, in "Proceedings of the International Conference on Duplex Stainless steels", edited by J. Charles and S. Bernhardsson, Vol. 1 (Les Editions de Physique, Paris, 1991) pp. 667–75.
6. S. TOSTO and F. NENCI, *Mem. Etudes Sci. Rev. Metall.* June (1987) 311.
7. J. NOORDHUIS and J. Th. M. DE HOSSON, *Acta Metall. Mater.* **41** (1993) 1989.
8. HU JIANDONG, *J. Mater. Sci.* **27** (1992) 671.
9. HU JIANDONG and LI ZHANG, *Mater. Sci. Technol.* **8** (1992) 796.
10. JIANGLONG LIU and QIQUAN LUO, *Mater. Lett.* **16** (1993) 134.
11. T. N. KIM and A. J. BOURDILLON, *Mater. Sci. Technol.* **8** (1992) 1011.
12. K. B. GUY, E. P. PUTLER and D. R. F. WEST, *Met. Sci.* **17** (1987) 167.

Received 8 November 1993
and accepted 26 April 1994